Transient Simulation of Heterojunction Photodiodes—Part II: Analysis of Resonant Cavity Enhanced Photodetectors

M. Selim Ünlü, *Member, IEEE*, Bora M. Onat, *Student Member, IEEE*, Yusuf Leblebici, *Member, IEEE*

***Abstract*—The high-speed response properties of resonant cavity enhanced (RCE) photodetectors have been investigated. The limitations on the high-speed performance of photodiodes and the advantages of RCE-detection are discussed. Transient response of heterojunction photodiodes under pulsed optical illumination has been simulated using the method described in Part I. Results on conventional AlGaAs/GaAs and RCE GaAs/InGaAs heterojunction p–i–n photodiodes are presented. For small area detectors, almost 50% bandwidth improvement along with a two-fold increase in efficiency is predicted for RCE devices over optimized conventional photodiodes. A nearly three-fold enhancement in the bandwidth-efficiency product was shown.**

I. Introduction

PROGRESS IN OPTICAL communications and processing requires simultaneous development in light sources, interconnects, and photodetectors. While optical fibers have been developed for nearly ideal links for optical signal transmission, semiconductors have become the technology of choice for optical sources and detectors. Photodetectors for today's high performance optical communication and signal processing systems must have high sensitivities, short response times, and low power consumption. There are a variety of semiconductor photodetectors with these performance characteristics [1], [2]. A large quantum efficiency, i.e., the probability of detecting incident photons, is another important property for high performance photodetectors. The quantum efficiency of conventional detector structures is governed by the absorption coefficient of the semiconductor material requiring thick active regions for high quantum efficiencies, especially for long-wavelength detection. However, reduced device speeds result from the long transit times required in devices with thick active regions. It is desirable to enhance the quantum efficiency without increasing the active layer thickness in order to optimize the gain-bandwidth product. This enhancement in the quantum efficiency can be achieved by integrating the semiconductor detector in an asymmetric Fabry–Perot cavity [3], [4].

The enhancement of the quantum efficiency in resonant cavity enhanced (RCE) detectors is derived from the increased amplitude of optical field inside a Fabry–Perot cavity under the resonant condition. In addition to enhancing the photosensitivity at the desired wavelength, RCE-detection also provides wavelength selectivity since the off-resonance wavelengths are rejected by the cavity [5]. In this paper, we will discuss the implications of RCE-detection on high speed performance. The RCE-detection scheme is applicable to most of the semiconductor photodetectors [3]–[10]. Although the following discussion is given for p–i–n photodiodes similar implications can be expected for other photodetector structures.

For very high speed detection, p–i–n photodiodes are one of the best candidates. If high overall gain is required, the electrical output from the p–i–n detectors can be amplified by high-speed low-noise electronic devices [11], [12]. The response speed of conventional p–i–n detectors is rapidly increasing, and impulse responses of 1 ps for such detectors appear to be possible [1]. In this manuscript, the high-speed response properties of RCE-detectors is analyzed in comparison with the conventional structures. For an accurate analysis of the high speed performance of photodetectors, the transient simulation method described in Part I was used to predict the response under optical pulse excitation. As discussed in Part I, the simulation is achieved by using a direct method circuit simulator to solve the one-dimensional time-dependent semiconductor equations [13]. A detailed analysis of the transient response of p–i–n photodetectors designed for maximum speed is presented along with results predicting drastic improvements in the gain-bandwidth product for RCE-detectors. Although the ideas presented here are applicable for all wavelength regions and material systems, they are more important for infrared (IR) detectors where the detector performance is limited by moderate absorption coefficients of commonly used semiconductor materials. The examples will be given for GaAs/(Al,In)GaAs material system.

We will first describe several important theoretical aspects of p–i–n detectors related to frequency response and sensitivity. The intrinsic limitations on the high speed response of conventional p–i–n detectors will then be presented. The improvement in the bandwidth-efficiency product through reducing the transit times by allowing absorption only in a thin layer embedded in the depletion region, and restoring the quantum efficiency by RCE-scheme will be discussed. This first order analysis will be followed by the discussion of the transient simulation results.

Manuscript received June 21, 1993; revised November 27, 1994. This work was supported by the National Science Foundation under Grant ECS-9309607.

M. S. Ünlü and B. Onat are with the Center for Photonics Research and Department of Electrical, Computer and Systems Engineering, Boston University, Boston, MA 02215 USA.

Y. Leblebici was with the Department of Electrical and Computer Engineering, University of Illinois at Urbana-Champaign. He is currently with the Electrical Engineering Department, Istanbul Technical University.

IEEE Log Number 9409162.

II. High Speed Properties of Heterojunction *P–I–N* Photodiodes

The most important limitations on the response speed of heterojunction p–i–n photodetectors are 1) drift (transit) time across the depleted region τ_{tr}, 2) the time it takes to charge and discharge the inherent and parasitic capacitances τ_{RC}, 3) the diffusion time for the carriers generated in the undepleted regions τ_{diff}, and 4) charge trapping at the heterojunctions τ_{trap} [1].

Conventionally, all of these individual time constants are summed to obtain an overall response time constant. The following, then, describes the temporal response of the detector.

$$\tau = \tau_{tr} + \tau_{RC} + \tau_{\text{diff}} + \tau_{\text{trap}}. \tag{1}$$

One has to normalize the individual time constants according to the fraction of the photogenerated carriers participating in the particular process. For example, although the diffusion time is a constant, the influence on the overall response speed will change drastically with the relative amount of light absorbed in the neutral contact regions. In short, different speed limitations should be carefully considered for a specific detector structure, if this semi-empirical approach is taken.

Charge trapping is especially important in waveguide photodetectors where a large bandgap discontinuity necessarily results from the requirement for large refractive index variation (different materials) in the waveguide design. In p–i–n type photodetectors, the speed limitation due to current diffusion out of absorbing neutral regions can be removed by using larger bandgap contact layers which are transparent at the excitation wavelengths. Therefore, the absorbing region is completely depleted, and neutral regions do not respond to the excitation. In such a configuration, to avoid charge trapping, the heterojunctions formed between the large bandgap neutral regions and the depleted absorbing layers need to be graded. If the heterointerface is positioned within the normally depleted region where a large electrical field exists under normal operating conditions, the charge storage at the heterojunctions can be almost entirely removed. In the following discussion, we neglect the speed limitations due to charge trapping and diffusion which can be eliminated by proper device design and concentrate on the intrinsic limitations imposed by the transit and capacitance charging times.

The transit time depends on the carrier velocities, v_e and v_h, for electrons and holes, respectively, and it is dominated by the slower carriers. In a conventional detector, photogenerated carriers have to traverse the entire depletion region (see Fig. 1(a)). The transit time lmited 3-dB bandwidth of a thin detector is given by

$$f_{tr} = 0.45\frac{v}{L} \tag{2}$$

where L is the depletion width, and v is the carrier velocity (the hole velocity for GaAs is around 6×10^6 cm/s). The transit time considerations suggest that very thin intrinsic layers are needed to achieve high-speed response. For instance, for 1 ps response, $L = 0.06\,\mu$m. However, as the intrinsic layer thickness is decreased, the capacitance increases and limits

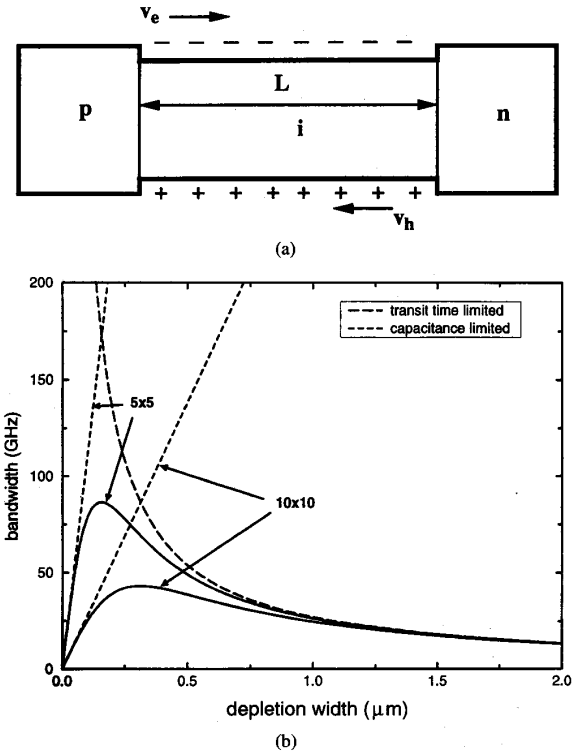

Fig. 1. (a) Schematic representation of a conventional heterojunction p–i–n photodetector illustrating the distances that the photogenerated carriers have to transit. (b) The bandwidth-depletion width dependence (solid lines) are shown for 10×10 and 5×5 μm^2 area conventional p–i–n detectors. The transit time limited bandwidth (dashed line) is common for different size devices and capacitance limited bandwidth (dotted lines for a total output resistance of 50 Ω) varies with the device area.

the bandwidth. The capacitance limited bandwidth is

$$f_{RC} = \frac{1}{2\pi R_T C} = \frac{L}{2\pi R_T \epsilon_r \epsilon_0 A} \tag{3}$$

where ϵ_r is the relative permittivity of the semiconductor ($\epsilon_r = 13$ for GaAs), A is the area of the device, and R_T is the total resistance (load resistance + contact resistance). As can be seen from (2) and (3), the dependence of the transit time and capacitance limited bandwidths on the depletion width L are inversely related, consequently, for any given detector area and load resistor there is an optimum intrinsic layer thickness that yields the maximum bandwidth. Fig. 1(b) shows the bandwidth of 10×10 and $5 \times 5 \mu$m^2 area conventional detectors as a function of depleted layer thickness for a total resistance of 50 Ω. The maximum bandwidth for this structure is reached at a 0.3 and 0.15 μm depleted layer thickness and are about 43 and 86 GHz for the larger and smaller device dimensions, respectively.

For a high speed detector, where the depletion width is small, i.e., $\alpha L \ll 1$ (α is the absorption coefficient), and absorption only takes place in the depleted region, the quantum efficiency is given by

$$\eta = (1 - R)(1 - e^{-\alpha L}) \approx (1 - R)\alpha L \tag{4}$$

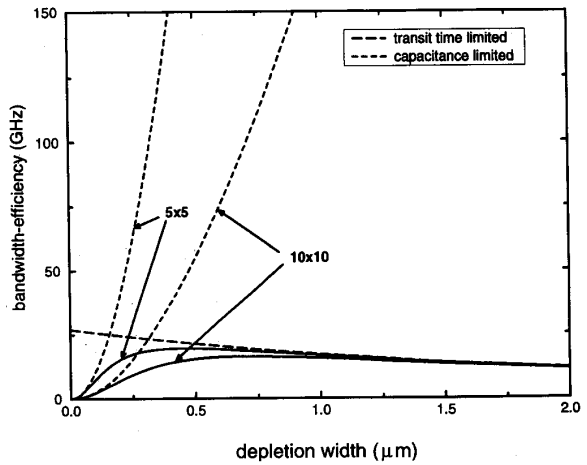

Fig. 2. Bandwidth-efficiency product versus the depletion (absorption) region width for conventional detectors as depicted in Fig. 1(a). The transit time and capacitance limitations are shown in dashed and dotted lines, respectively.

and for an ideal anti-reflection coating, i.e., the top reflectivity, $R = 0$,

$$\eta \approx \alpha L. \tag{5}$$

Note that, the quantum efficiency increases with the thickness contrary to the transit time limited bandwidth. At the optimum bandwidth of the larger device shown in Fig. 1(b) ($L = 0.3\,\mu$m), $\eta \leq 0.26$. The increasing dependence of the sensitivity on the depletion width results in an optimum bandwidth efficiency product shifted toward larger thicknesses as shown in Fig. 2. The maximum value of the bandwidth-efficiency product for a 10×10 μm^2 GaAs detector with $R_T = 50\,\Omega$ is 16.2 GHz and occurs at $L = 0.7$ μm. The maximum bandwidth-efficiency product of the smaller device is only slightly higher than the larger device despite the significant difference in their maximum bandwidths (Fig. 1(b)).

The inverse relation of transit time limited bandwidth (2) with thickness suggests that infinitely large bandwidths can be achieved by decreasing the depletion width if the capacitance limitation is relaxed by shrinking the device area or reducing the total resistance. However, when we consider the bandwidth-efficiency product for a thin detector with no capacitance limitation, we obtain from (2) and (4)

$$f_{3dB} \cdot \eta = f_{tr} \cdot \eta = 0.45 \alpha v_h (1 - R) \tag{6}$$

which is independent of the design parameters and can be perceived as the y-intercept of the dashed line in Fig. 2. For anti-reflection coated ($R = 0$) GaAs detectors ($\alpha \approx 10^4$ cm^{-1}, $v_h = 6 \times 10^6$ cm/s) this product is 27 GHz.

Alternatively, the quantum efficiency of thin p–i–n detectors can be improved by collecting the light through the mesa edge of the device, perpendicular to the electrical current. This configuration provides a long absorption region and a short current path simultaneously, enabling the independent optimization of high speed and high efficiency properties. In this waveguide configuration, however, the collection efficiency for the incoming light limits the overall quantum efficiency. Furthermore, the waveguide design suffers from charge trapping at the heterojunctions between the cladding layers and the active regions. The band discontinuities at the heterojunctions can not be selected to be arbitrarily small since the confinement factor Γ is heavily influenced by the difference in the refractive index which in turn gives the effective absorption coefficient as $\Gamma\alpha$. Moreover, coupling the light into a very thin (< 1 μm) region is a major technological difficulty. Resonant cavity enhanced detection provides high sensitivity without requiring a thick absorption region or complicated coupling schemes.

In the following section we will discuss the high-speed response implications of the RCE-detection. Since high quantum efficiency can be maintained for thin detector structures ultra high bandwidth efficiency products can be realized.

III. High Speed Performance of Resonant Cavity Enhanced Photodetectors

In the RCE photodetectors, the detection region is integrated into an asymmetric Fabry–Perot cavity formed by two mirrors (top and bottom), and at the resonance condition, the incoming light interferes constructively with the reflected component from the bottom mirror. The resulting resonant cavity effect enhances the internal optical field amplitudes at the resonant wavelengths [4]. For a high quality factor Q cavity (high mirror reflectivities and a thin absorption region), a drastic increase in η can be obtained. Therefore, a high η detection can be achieved even for a very thin (fractions of a micron or less) active layer allowing for a detector design with a thin absorber embedded in the depletion region without sacrificing the detector sensitivity. Resonant cavity enhancement can also be viewed as a multiple-pass detection over a thin absorbing region. The mirrors and contact layers should be formed using larger bandgap materials to eliminate any absorption at the operation wavelength to ensure high Q. Only the absorption region is made of a smaller bandgap material which absorbs at the wavelengths of interest. Resonant cavity enhanced (RCE) detectors having such a multiple-pass detection scheme were demonstrated with AlGaAs/GaAs heterojunction phototransistors (HPT) [3], and with GaInAs/AlInAs Schottky photodiodes [6]. The former devices possess high quantum efficiencies of 43% for a very thin active layer of only 0.1 μm. Several other devices employing the RCE-detection such as GaAs/InGaAs avalanche photodiodes [7], HPT's in InGaAlAs/InGaAs/InP [8], and metal-semiconductor-metal (MSM) detectors in AlGaAs/GaAs [9] have also been realized.

An expression for the peak quantum efficiency of RCE photodetectors can be obtained for given top and bottom mirror reflectivities R_1 and R_2, respectively, and an active region of thickness d and absorption coefficient α [4].

$$\eta_p = \left\{ \frac{(1 + R_2 e^{-\alpha d})}{(1 - \sqrt{R_1 R_2} e^{-\alpha d})^2} \right\} \times (1 - R_1)(1 - e^{-\alpha d}). \tag{7}$$

where R_1 and R_2 are the magnitude of mirror reflectivities. The phase angles of mirror reflectivities should be considered

to achieve the resonance condition. The cavity can be tuned by recessing a sacrificial layer as discussed in [2], [3]. In the limit of a thin active layer, i.e., $\alpha d << 1$, η_p is:

$$\eta_p \simeq \left\{ \frac{(1+R_2(1-\alpha d))}{(1-\sqrt{R_1R_2}(1-\alpha d))^2} \right\} \times (1-R_1)\alpha d. \quad (8)$$

If the thickness of the active region is smaller than half the wavelength of the light, one should also consider the influence of the standing wave pattern inside the resonant cavity [10]. Resonant cavity enhancement can be applied in any semiconductor detector structure. In this paper, we consider a p–i–n detector placed in such a resonant cavity and investigate its high speed performance. As discussed below, not only the sensitivity of this RCE-pin structure but also its bandwidth is superior to its conventional counterpart.

We consider a p–i–n detector structure which has a smaller bandgap absorption region of thickness d placed in a depletion region of L as shown in Fig. 3(a). We refer to this structure as the RCE-detector, since the resonant cavity enhancement allows for optimizing the depletion and absorption regions separately. In this case, the carriers do not have to traverse the entire depletion region. The transit times, τ_e and τ_h, for electrons and holes, respectively, are given by

$$\tau_e = \frac{L_1}{v_e} \quad \text{and} \quad \tau_h = \frac{L_2}{v_h}. \quad (9)$$

The transit time is optimized when $\tau_e = \tau_h$. From Fig. 3(a),

$$L + d = L_1 + L_2 \quad (10)$$

and therefore, the optimized transit time limited bandwidth for the RCE-detectors is

$$f_{tr} = 0.45\frac{v_h + v_e}{d+L} \qquad \text{for} L > d \quad (11)$$

which represents a drastic improvement over conventional detectors (2) since in most compound semiconductors $v_e > v_h$ (for example, $v_e \approx 1 \times 10^7$ cm/s in GaAs). The capacitance limited bandwidth remains unchanged with the RCE-design and it is only related to the depletion width and device area as given by (3). Fig. 3(b) shows the dependence of bandwidth on the depletion width L for 10×10 and $5 \times 5 \mu m^2$ area GaAs RCE-detectors with a 0.1-μm-thick absorption region. When compared with the bandwidth of the conventional detector (Fig. 1), we see that the optimum bandwidth moves toward thicker depletion regions and a maximum of 64 GHz is reached at $L = 0.5$ μm for the larger device, and maximum bandwidth approaches 120 GHz (at $L = 0.25$ μm) for the smaller device.

Using the RCE-scheme, a large quantum efficiency can be maintained independent of the depletion width. Using the peak quantum efficiency relation (7), we obtain $\eta = 0.9$ for a 0.1-μm-thick absorber ($\alpha d = 0.1$) with $R_2 = 0.99$ and $R_1 = 0.7$, and this η remains unchanged as long as $L > d = 0.1$ μm. When $L < 0.1$ μm, η needs to be evaluated by replacing d with L in (7). The bandwidth efficiency product evaluated under these constraints for the RCE-pin is shown in Fig. 4. The maximum bandwidth-efficiency product of 58 GHz for the 10×10 μm^2 RCE-pin represents a more than 3.5-fold improvement over the conventional detector (16.2 GHz) For the $5 \times 5 \mu m^2$ device this predicted improvement is more drastic, over a five-fold increase from 19 to 106 GHz.

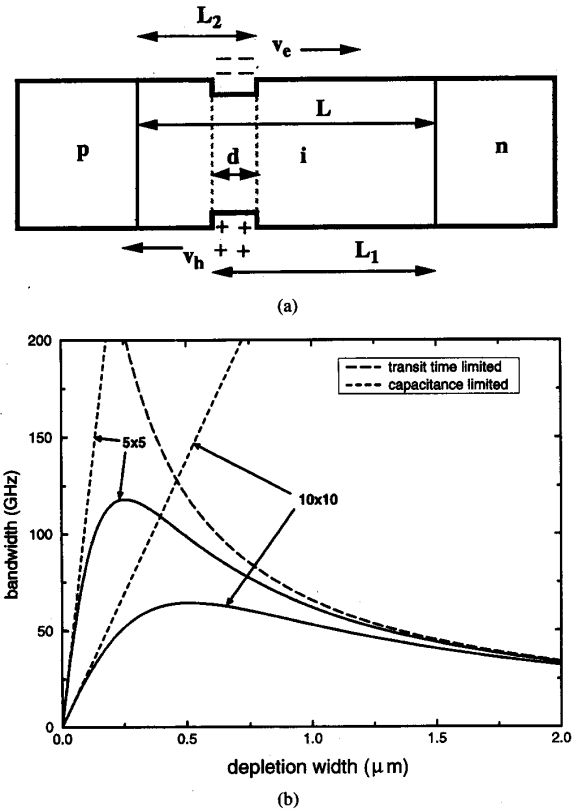

Fig. 3. (a) Schematic representation of a p–i–n photodetector optimized for RCE-detection in a thin layer illustrating the distances that the photogenerated carriers have to transit. (b) The bandwidth-depletion width dependence (solid lines) are shown for 10×10 and 5×5 μm^2 area RCE p–i–n detectors. The transit time limited bandwidth (dashed line) is common for different size devices and capacitance limited bandwidth (dotted lines for a total output resistance of 50 Ω) varies with the device area.

In the above discussion, we presented the bandwidth considerations for 10×10 and $5 \times 5 \mu m^2$ device sizes. As the device size is reduced, the capacitance limitation shifts toward thinner depletion regions. At this extreme, the influence of the RCE-scheme is even more prominent since the intrinsic limitation on the bandwidth-efficiency product (6) is relaxed by removing the direct dependence of the quantum efficiency on the depletion layer thickness.

For the high-speed response of the RCE-detectors, we should also consider the photon lifetime in the optical cavity as one of the limiting factors. The photon lifetime τ_p can be viewed as the time required to build or decay the optical fields inside the cavity and is given by [14]

$$\tau_p = \frac{\tau_{RT}}{1 - R_1R_2\exp(-2\alpha d)} \quad (12)$$

where τ_{RT} is the time required for photons to make one round trip in the optical cavity, and the denominator is the total decay they encounter during this round trip. For a 1μm long GaAs cavity, $\tau_{RT} = 23$ fs. For the cavity described above ($R_1 = 0.7$, $R_2 = 0.99$, $d = 0.1$ μm), τ_p is around 50 fs which

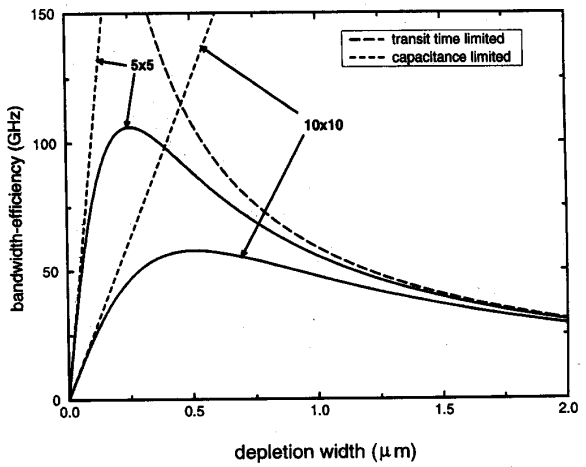

Fig. 4. Bandwidth-efficiency product versus the depletion (absorption) region width for RCE detectors as depicted in Fig. 3(a). The transit time and capacitance limitations are shown in dashed and dotted lines, respectively.

is much smaller than the carrier drift time. Even for RCE-detectors with thinner absorbers ($d \approx 0.05\,\mu$m) and higher reflectivity mirrors ($R_1 > 0.9$) the τ_p remains in the order of 100 fs. Therefore, the photon lifetime will be an important factor only for detectors designed for THz operation and can be neglected for detectors with response times in excess of 1 ps.

We presented simplistic pictures for the bandwidths for conventional and RCE-detectors which neglect diffusion of carriers under electrical field and assume a pure drift. We also neglected the electric field dependence of mobility, recombination, and the influence of heterojunctions. Under these assumptions, we can also predict the impulse response of photodiodes. The current $i(t)$ due to a carrier of charge Q moving with a velocity of $v(t)$ in a semiconductor material of thickness L is given by [15]

$$i(t) = -\frac{Q}{L}v(t). \tag{13}$$

Fig. 5 shows a comparison of the theoretical current responses for conventional and RCE p–i–n photodetectors. For a single electron-hole pair generated in the middle of the depletion region the current is given by Fig. 5(b). For the conventional detector, under uniform photogeneration, the transit-time spread is more severe since the full-width of the time spread is determined by the slower carriers (holes) traversing the farthest distance (Fig. 5(c)). The transit-time spread for the RCE-detectors can be minimized by the proper selection of the absorption region as discussed above. Under this constraint the theoretical current response is uniform with a small time spread as shown in Fig. 5(d).

A brief inspection of Fig. 5(c) and (d) reveals very different temporal response for conventional and RCE p–i–n detectors. Therefore, a comparison of the bandwidths of these detectors, solely considering the maximum transit time, as presented above (Figs. 1 and 3), is not accurate. A better first order comparison can be obtained by evaluating the Fourier transforms of the corresponding temporal impulse responses. Fig.

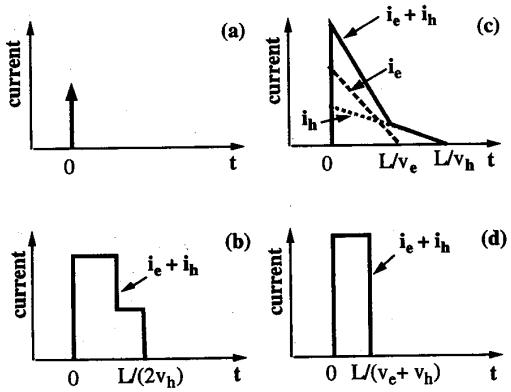

Fig. 5. The theoretical current response of a photodetector with a depletion region width of L when excited by an optical impulse under constant drift velocity and no diffusion assumption. The vertical scales are arbitrary, and the horizontal scales are intended for a qualitative comparison of different cases. (a) The optical impulse arriving at $t = 0$. (b) The current for a single electron-hole pair generated in the middle of the depletion region. The response continues until the hole reaches the contact. (c) The current for a conventional structure with uniform generation across the depletion region. The response lasts until the holes generated at the opposite end traverse the entire depletion region. (d) The current for an optimized RCE detector. The electrons and holes arrive at the contacts at the same time.

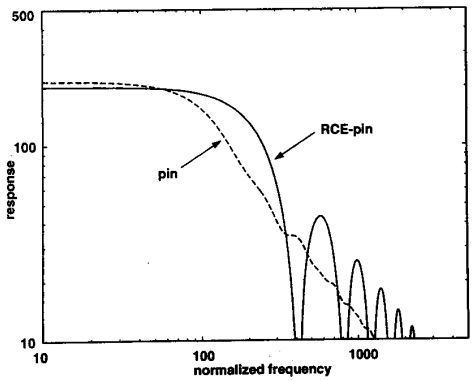

Fig. 6. Frequency domain representation of the impulse responses of conventional and RCE-detectors as shown in Fig. 5(c) and (d), respectively. The axes are in arbitrary units and intended for a relative comparison. A hole to electron drift velocity ratio of 0.6 is assumed.

6 shows the frequency response for the currents depicted in Fig. 5(c) and (d). On a normalized scale, frequency response of RCE-pin extends to higher frequencies in comparison with its conventional counterpart. The 3-dB bandwidth is approximately 70% higher for the RCE-pin which is comparable to that is predicted by the simplistic approach presented by (2) and (11), and it is a very drastic increase. Moreover, RCE-detection goes beyond simply restoring the quantum efficiency and offers higher detector sensitivity resulting in a double faceted enhancement in bandwidth-efficiency product.

When photodetectors with picosecond response times are considered, a more accurate representation of the transient response is desirable. In Part I of this paper, we discuss the time dependent solution of the device equations and its application to predict the temporal response of photodetectors under pulsed illumination. Below, we present the application

of this method to the comparison of conventional and RCE p–i–n photodiodes.

IV. Simulation Results on RCE and Conventional Heterojunction Photodiodes

For comparison of the conventional and RCE detectors, we have selected two heterojunction p–i–n photodiode structures. These structures follow the design rules suggested in the above given discussions for highest performances. The intrinsic region is assumed to be lightly n-doped and its width is selected to be 0.72 μm corresponding to the maximum bandwidth-efficiency product condition for a 10×10 μm^2 conventional p–i–n diode. This depletion width is slightly larger than the optimum value for the RCE-detector. Therefore, this selection favors the conventional structure.

The conventional device which we modeled (#1) has a 0.64 μm thick, normally depleted n^--GaAs absorbing region and $Al_{0.06}Ga_{0.94}As$ contact (or window) layers. The schematic diagram of the device is shown in Fig. 7(a). The AlGaAs contact layers allow for high speed operation by removing the limitation imposed by the current diffusion out of absorbing but undepleted regions which is a slow process. Within a wavelength range (825 nm $< \lambda \leq$ 870 nm) determined by the absorption edge of the AlGaAs and GaAs layers, photogeneration will occur only in GaAs regions ($\alpha = 10^4$ cm^{-1}). The carriers that may be generated in the GaAs substrate and cap layers are blocked by the AlGaAs barriers, i.e., they do not contribute to the photocurrent, and thus the device speed is limited solely by the transit time of photogenerated carriers across the 0.72 μm depletion region. A small Al mole fraction was chosen to avoid large band discontinuities. The heterojunctions were graded and positioned inside the depletion region to prevent charge trapping. The total band discontinuity is 75 meV, 1/3 of which is assumed to be at the valence band. For this conventional detector structure, we assume a nearly ideal anti-reflection coating (surface reflectivity $\simeq$ 0.05) resulting in a quantum efficiency of 0.45 from (4) within the 825–875 nm wavelength range.

The RCE photodiode structure (#2) has GaAs contacts (p and n) and depletion regions (Fig. 7(b)). A 0.08-μm-thick $In_{0.07}Ga_{0.93}As$ absorption region is placed in the depletion region extending the wavelength sensitivity spectrum of the detector to 920 nm. Within a wavelength range of 870 to 920 nm, only this InGaAs region absorbs ($\alpha = 10^4$ cm^{-1}) incident light and the remainder of the detector is transparent. The position of the absorbing layer is optimized according to the relative carrier velocities for electrons and holes. For this optimization, we first run the device simulation with no optical excitation and calculate the electron and hole mobilities in the depletion region for the electrical bias to be used for transient analysis. These mobilities were used to evaluate the ratio of electron and hole velocities and thus the position of the absorption region for the fastest detector response. As a result, the distance of the absorption layer from the p-region is approximately half of that from the n-region.

We consider a Fabry–Perot resonant cavity formed by an ideal bottom mirror ($R_2 \simeq 1.0$) and a high reflectivity ($R_1 =$ 0.7) top mirror. The quantum efficiency of this RCE-detector is estimated at $\eta = 0.9$ at wavelengths around 900 nm. The electrical contacts are assumed to be between the multilayer mirrors to prevent high resistances. Since the current does not flow through the mirror regions, the large band discontinuities required for the mirror formation does not effect the electrical performance. The photoresponse of these two structures (#1 and #2) are calculated accurately using the one dimensional transient simulation method we have developed (Part I).

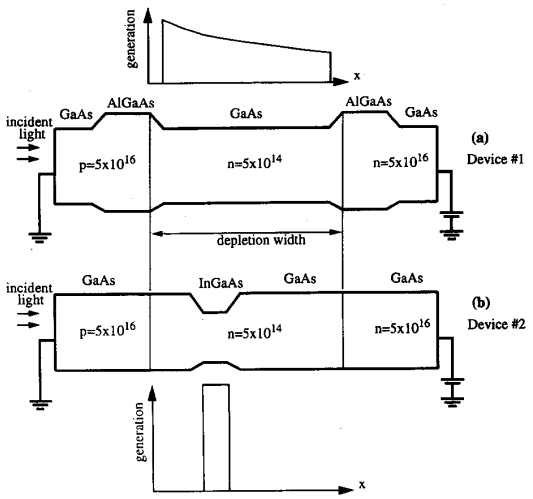

Fig. 7. The schematic flat band diagram (applied and built-in fields are not shown) of the modeled p–i–n photodiodes and the qualitative representation of the photogeneration terms. (a) Device #1: the conventional AlGaAs/GaAs p–i–n heterojunction photodiode. The photogeneration occurs in the depleted GaAs region on an exponentially decaying profile. (b) Device #2: the GaAs RCE photodiode with an InGaAs absorbing region. The generation is localized in the InGaAs region. The band discontinuities are exaggerated to clearly identify the graded regions.

Figs. 8 and 9 illustrate the time evolution of the hole $p(x,t)$ and electron $n(x,t)$ concentrations, respectively, for the InGaAs/GaAs heterojunction photodiode structure (Device #2, Fig. 7) described above. Steady state carrier distributions, as can be observed at $t = 0$, clearly shows the depletion region and the location of heterojunctions. The wavelength of the optical excitation was chosen so that photogeneration would occur in the InGaAs region only. The optical excitation is a square pulse of about 9×10^{14} photons/device for a 10×10 μm^2 device ($\approx$180 W/cm^2) with negligible rise and fall times (0.01ps) and a full-width-at-half-maximum (FWHM) of about 10 ps. We assume that 90% of the incident photons are absorbed in the thin InGaAs region. Such a high quantum efficiency can be achieved using the RCE-detection scheme [3], [4].

The transient variation of electron and hole variations (Figs. 8 and 9) reveal the advantages of the design with a thin absorbing layer embedded in the depletion region. Both electrons and holes are swept under the electrical field in the depletion region immediately after photo-generation. Carrier diffusion into the neutral regions is negligible and the carrier concentrations return to their steady state values shortly after the termination of optical excitation. Fig. 10 shows the short

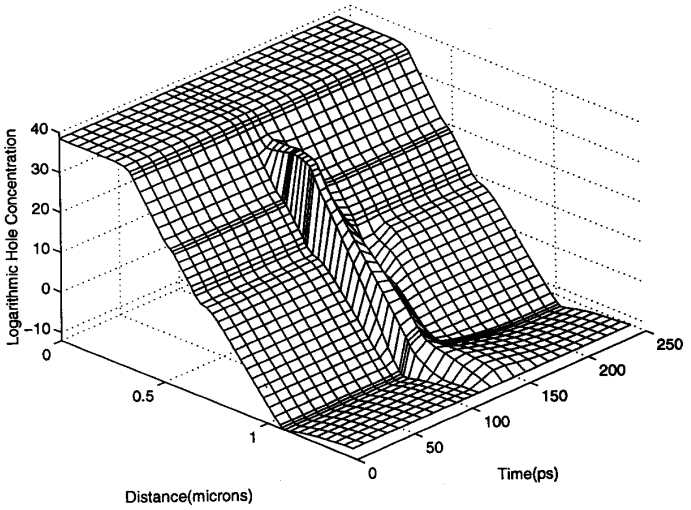

Fig. 8. Simulated variation of hole concentration in the InGaAs/GaAs p–i–n diode (Device #2) as a function of time and position when light is absorbed across the depletion region. The steady state hole distribution can be observed at $t = 0$.

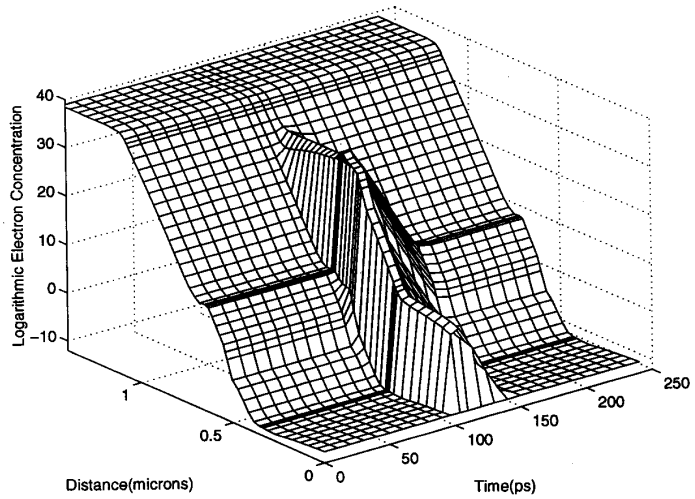

Fig. 9. Simulated variation of electron concentration in the InGaAs/GaAs p–i–n diode (Device #2) as a function of time and position when light is absorbed across the depletion region.

circuit photocurrent response of the same photodiode (Device #2). The time variation of the displacement and conduction current components are illustrated in comparison with the generation term. Since there are no assumptions and approximations in the time variation of the semiconductor equations in the presented model, the calculated current is an accurate representation under large pulse excitation. With the increasing speed of photodetectors such accurate models will become necessary tools.

The ultimate response time of photodetectors can be determined by observing their transient current under optical pulses of varying duration. Within the convergence capabilities of the circuit simulator we have utilized, it is possible to calculate the output current for an optical pulse of less than 1 ps FWHM. Since the estimated transit time for conventional and RCE device designs are about 5 to 10 ps, we compare the transient response of the two devices under a 5 ps optical pulse. To ensure small signal condition, pulse amplitude was chosen as 1% of the previous example (Figs. 8–10). Fig. 11 shows the simulated short circuit currents for the conventional (dashed line) and RCE (solid line) p–i–n detectors under a 5 ps FWHM optical pulse. At first glance, we observe a larger (magnitude) and sharper (less time spread) current for the RCE-detector compared to the conventional case.

A close inspection of the individual current components reveals the expected transient features and superiority of the RCE-detector.

1) The rise and fall times of the total current are comparable for the RCE design. For the conventional detector, the

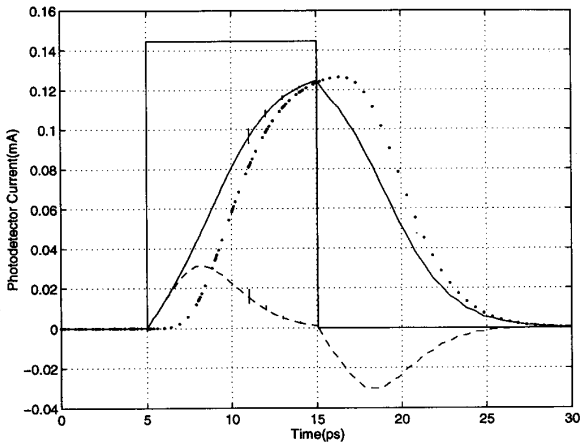

Fig. 10. The short circuit current output evaluated for the simulation example shown in Figs. 8 and 9 (time axis is re-scaled for clarity). The photogeneration term, and displacement (dashed line) and conduction (dotted line) current components are illustrated.

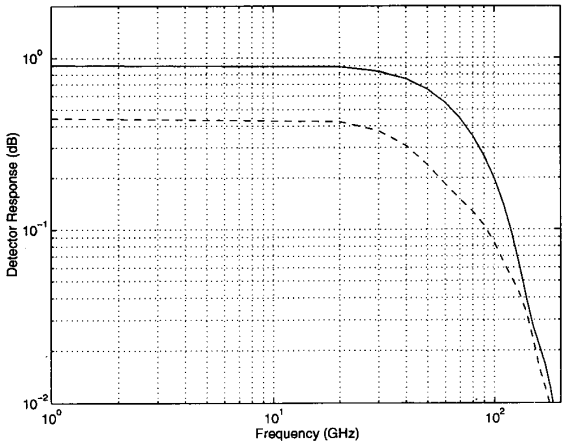

Fig. 12. Frequency response of conventional (dashed) and RCE (solid line) p–i–n photodetectors obtained by Fourier transform of pulse responses shown in Fig. 11. The optical excitation term was deconvolved to extract the impulse response.

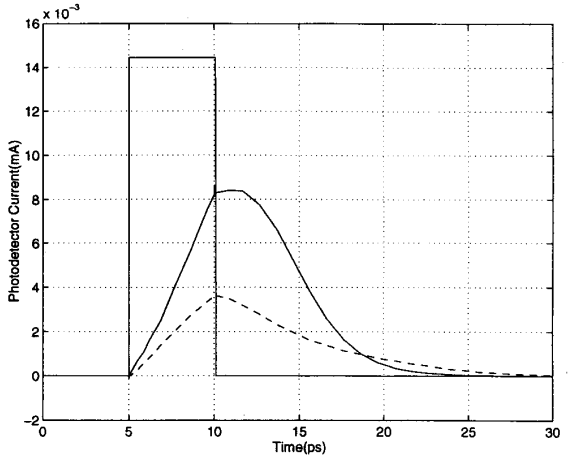

Fig. 11. The transient short circuit photocurrent under a 5 ps FWHM optical pulse for AlGaAs/GaAs conventional p–i–n (Device #1, dashed line), and GaAs/InGaAs RCE detector (Device #2, solid line).

fall time is much larger than the rise time as a result of long transit time for holes.

2) The RCE-detector not only has larger current under identical optical excitation owing to the enhanced quantum efficiency, but also the response is faster than the conventional counterpart. Therefore, the bandwidth-efficiency product is doubly improved by the RCE-detection scheme.
3) Due to the simultaneous arrival of both kinds of carriers at the contacts, the time spread of the conduction current for the RCE design is much smaller than the conventional p–i–n in which the carriers reach the contacts at different times determined by the position of the photogeneration.

For a comparison of the RCE and conventional detectors in the frequency domain, we used Fast-Fourier-Transform (FFT). The simulated temporal responses depicted in Fig. 11 were converted into frequency domain by FFT and shown in Fig. 12. Fourier analysis of the optical excitation term gives a flat spectrum (within 1dB) up to approximately 100 GHz verifying the accuracy of the frequency domain representation of the current pulses. Furthermore, to eliminate the influence of the finite width of the optical excitation pulse, it was deconvolved from the simulated current responses. From Fig. 12, the transit time limited 3-dB bandwidth of the conventional p–i–n detector can be calculated as 52 GHz in comparison with 70 GHz for the RCE-pin, corresponding to a 35% improvement. This improvement is less than the 70% value calculated for the idealized impulse responses as shown in Figs. 5 and 6. This difference is due to two reasons. First, the generation region in the RCE-pin is of finite thickness resulting in a slight variation of the arrival of photogenerated carriers at the contacts. Secondly, and more importantly, diffusion of carriers can not be neglected (as it was in the simplistic case) even in the depletion region. We have further verified that the diffusion is the dominant effect by varying the thickness of the generation region in the RCE-pin and observing the temporal shape of the current pulse.

When we compare the transit time limited bandwidth-efficiency products of the two structures we see a drastic improvement. For the conventional p–i–n, BWE is 23 GHz, which is slightly smaller than the theoretical limit based on the transit time of holes. The BWE of the RCE-pin is 63 GHz which represents a nearly three-fold improvement. If the optimum depletion width for RCE detector is considered ($L \sim 0.5\,\mu$m) then the BWE can be extended to 100 GHz.

For a direct comparison of the bandwidths for RCE and conventional p–i–n structures, we plot the peak value of the normalized short circuit current (or detector response) as a function of the inverse pulse FWHM (Fig. 13). When the pulse duration is large, the output current reaches its maximum value determined by the internal quantum efficiency, i.e., $\eta = 0.45$ for conventional and $\eta = 0.9$ for RCE detectors. As the optical pulse width becomes smaller, the electrical current is unable to

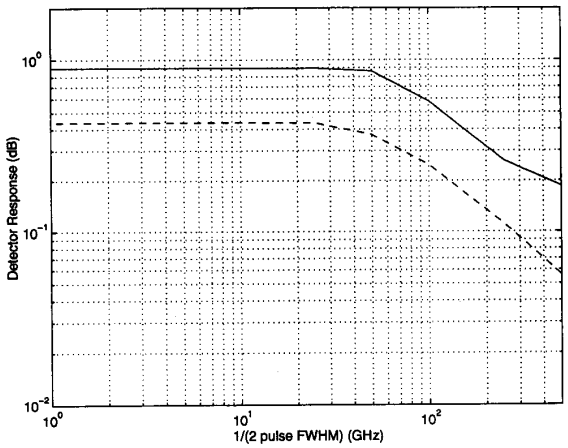

Fig. 13. Detector response (peak value of the normalized detector current) versus the inverse excitation pulse width for conventional (dashed) RCE (solid line) p–i–n detectors.

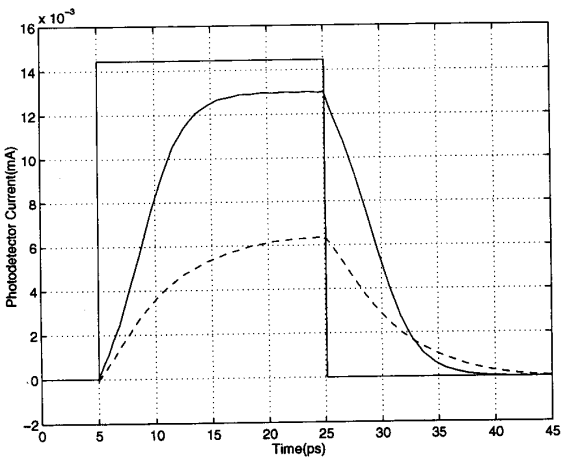

Fig. 14. The transient short circuit photocurrent under a long optical pulse with 0.01 ps fall time for conventional (dashed) and RCE (solid) p–i–n detectors. The excitations is long enough to allow both devices to reach their steady state current levels.

reach the steady state value. Although the ratio of electron hole pairs to the number of incident photons remains the same, the peak current decreases since the current is spread over time. The peak short circuit current drops to half of its maximum at a pulse FWHM of 4.5 and 3.5 ps for conventional and RCE p–i–n detectors, respectively. Therefore, the bandwidth of the RCE p–i–n is approximately 30% larger than that of the conventional diode (see Fig. 13) confirming our findings through Fourier analysis. Note that, both of these comparisons are made for a single optical pulse of varying duration. If we consider repetitive pulses, or sinusoidal excitation, the bandwidth difference will be even larger due to the large fall time of the conventional p–i–n.

To this end, we also compare the fall times for RCE and conventional p–i–n diodes. We calculated the response of these devices (Devices #1 and #2) under a long optical pulse such that both devices can reach the steady state current levels. The optical pulse is terminated abruptly (fall time= 0.01 ps) and we observe the decay of the short circuit current for both cases as shown in Fig. 14. Despite the higher steady state level, the current from the RCE detector decays faster and drops to lower values than the current for the conventional p–i–n. We have computed the fall time τ_f as the time it takes the current output to drop from 90% to 10% of the steady state value. The fall time $\tau_f = 7.1$ ps for the RCE p–i–n is 60% of that for the conventional structure ($\tau_f = 11.7$ ps) corresponding to 65% faster response.

V. Conclusion

A drastic improvement in the high-speed performance of heterojunction photodiodes is predicted using the resonant cavity enhanced (RCE) detection scheme. Since the RCE-detection allows for very thin absorption layers without sacrificing the quantum efficiency, p–i–n detector structures with thin absorbers embedded in the depletion region can be designed. A detailed analysis of the limitations on the high-frequency response of p–i–n detectors and the implications of the RCE-detection were presented. The transient responses of conventional and RCE photodiodes are accurately calculated under pulsed optical excitation. The excitation pulse width was varied and response to pulses as short as 1 ps FWHM was simulated. Fourier analysis was used for comparison in the frequency domain.

The simulation results demonstrated a 35% bandwidth improvement along with a two-fold enhancement in quantum efficiency over conventional p–i–n photodiodes optimized for a 10×10 μm^2 device area. For smaller area devices, even more drastic improvements exceeding a three fold increase in the bandwidth-efficiency product can be achieved. Our simulation results suggest that high quantum efficiency RCE-photodetectors can be realized with bandwidth-efficiency products approaching 100 GHz.

References

[1] J. E. Bowers and C. A. Burrus, Jr., "Ultrawide-band long-wavelength p–i–n photodetectors," *J. Lightwave Technol.*, vol. 5, pp. 1339–1350, 1987.

[2] R. G. Hunsperger, *Integrated Optics: Theory and Technology*. New York: Springer-Verlag, 1991.

[3] M. S. Ünlü, K. Kishino, J. I. Chyi, J. Reed, S. N. Mohammad, and H. Morkoç, "Resonant cavity enhanced AlGaAs/GaAs heterojunction phototransistors with an intermediate InGaAs region in the collector," *Appl. Phys. Lett.*, vol. 57, pp. 750–752, 1990.

[4] K. Kishino, M. S. Ünlü, J. I. Chyi, J. Reed, L. Arsenault, and H. Morkoç, "Resonant cavity enhanced (RCE) photodetectors," *IEEE J. Quantum Electron.*, vol. 27, pp. 2025–2034, 1991.

[5] M. S. Ünlü, K. Kishino, J. I. Chyi, L. Arsenault, J. Reed, and H. Morkoç, "Wavelength demultiplexing heterojunction phototransistors," *Electron. Lett.*, vol. 26, pp. 1857–1858, 1990.

[6] A. Chin and T. Y. Chang, "Multilayer reflectors by molecular beam epitaxy for resonance enhanced absorption in thin high-speed detectors," *J. Vac. Sci. Technol. B*, vol. 8, pp. 339–342, 1990.

[7] R. Kuchibhotla, A. Srinivasan, J. C. Campbell, C. Lei, D. G. Deppe, Y. S. He, and B. G. Streetman, "Low-voltage high-gain resonant-cavity avalanche photodiode," *IEEE Photon. Technol. Lett.*, vol. 3, pp. 354–356, 1991.

[8] A. Dodabalapur and T. Y. Chang, "Resonant-cavity InGaAlAs/InGaAs/InAlAs phototransistors with high gain fro 1.3–1.6 μm," *Appl. Phys. Lett*, vol. 60, pp. 929–931,1992.

[9] Z.-M. Li, D. Landheer, M. Veilleux, D. R. conn, R. Surridge, J. M. Xu, and R. I. Mcdonald, "Analysis of a resonant-cavity enhanced GaAs/AlGaAs MSM photodetector," *IEEE Photon. Technol. Lett.*, vol. 4, pp. 473–476, 1992.
[10] M. S. Ünlü, K. Kishino, H. J. Liaw, and H. Morkoç, "A theoretical investigation of resonant cavity enhanced photodetectors with Ge and Si active regions," *J. Appl. Phys.*, vol. 71, pp. 4049–4058, 1992.
[11] M. Brain and T. P. Lee, "Low-Noise optical receiver for high-speed optical transmission," *J. Lightwave Technol.*, vol. LT-3, pp. 1281–1300, 1985.
[12] S. Chandrasekhar, A. G. Dentai, C. H. Joyner, B. C. Johnson, A. H. Gnauck, and G. J. Qua, "4 Gbit/s pin/HBT monolithic photoreceiver," *Electron. Lett.*, vol. 26, pp. 1880–1882, 1990.
[13] Y. Leblebici, M. S. Ünlü, H. Morkoç, and S. M. Kang, "One-dimensional transient device simulation using a direct method circuit simulator," in *Proc. IEEE Int. Symp. Circ. Syst.*, 1992, pp. 895–898.
[14] J. T. Verdeyen, *Laser Electronics*, 2nd Ed. Englewood Cliffs, NJ: Prentice Hall, 1989.
[15] B. E. A. Saleh and M. C. Teich, *Fundamentals of Photonics*. New York: Wiley, 1991.

M. Selim Ünlü (S'90–M'92), for a photograph and biography, see this issue, p. 405.

Bora M. Onat (S'92), for a photograph and biography, see this issue, p. 405.

Yusuf Leblebici (S'88–M'91), for a biography, see this issue, p. 405.